

Role of waveguide geometry in graphene-based electro-absorptive optical modulators

This content has been downloaded from IOPscience. Please scroll down to see the full text.

2015 J. Phys. D: Appl. Phys. 48 355102

(<http://iopscience.iop.org/0022-3727/48/35/355102>)

View [the table of contents for this issue](#), or go to the [journal homepage](#) for more

Download details:

IP Address: 141.35.40.157

This content was downloaded on 18/11/2015 at 12:37

Please note that [terms and conditions apply](#).

Role of waveguide geometry in graphene-based electro-absorptive optical modulators

Uroš Ralević^{1,2}, Goran Isić¹, Borislav Vasić¹, Dejan Gvozdić² and Radoš Gajić¹

¹ Center for Solid State Physics and New Materials, Institute of Physics, University of Belgrade, Pregrevica 118, 11080 Belgrade, Serbia

² Faculty of Electrical Engineering, University of Belgrade, Bulevar Kralja Aleksandra 73b, PO Box 35-54, 11120 Belgrade, Serbia

E-mail: uros@ipb.ac.rs

Received 2 March 2015, revised 29 June 2015

Accepted for publication 9 July 2015

Published 6 August 2015



Abstract

We investigate the variation of the graphene-waveguide coupling strength G , whose magnitude is the crucial parameter of efficient graphene-based electro-absorptive optical modulators, with the waveguide geometry and its graphene coverage. By sweeping a wide geometrical parameter space, we show that G can be improved up to few times by optimising the waveguide width and height. We find that the high values of G cannot be simply related to the modal confinement factor and assess the impact of a small detachment of graphene from vertical waveguide boundaries. Using perturbation theory, we demonstrate that the modulation depth to the insertion loss ratio of a graphene-based modulator is always independent of the geometry and determined by the residual conductivity of graphene.

Keywords: waveguides, graphene, electro-optical modulators

(Some figures may appear in colour only in the online journal)

1. Introduction

Graphene, the recently discovered two-dimensional allotrope of carbon [1], has several distinct properties that make it very attractive for optical modulators: it exhibits a strong interaction with light [2], optical transitions [3, 4] tunable by means of the electric-field effect [1], high mobility of charge carriers [5], low switching energies [6] and compatibility with many of the existing photonic devices [7–15]. Various geometries and material systems have recently been considered [16–19] for coupling with graphene. However, the silicon-on-insulator (SOI) platform offers compact optical waveguides which are the key components of various types of photonic integrated circuits [20, 21]. For these reasons, electro-optical modulators based on graphene coupled to SOI waveguides have been drawing most of the interest recently [22–30].

The working principle of the proposed electro-absorptive modulators relies on tunable interband transitions in graphene

[22]. A pristine graphene layer deposited on top of a waveguide absorbs the optical signal propagated in the waveguide as electrons in graphene are accelerated by the high-frequency electric field and undergo interband transitions. When, however, a gate voltage is applied, it raises the Fermi energy E_F in graphene which fills up the higher electronic levels, thus Pauli blocking interband transitions [3, 4]. It implies that the modulation depth achievable by changing the gate voltage increases linearly with the length L of the waveguide segment covered by graphene [28]. As the increase of L implies higher power consumption and a larger device footprint, it follows that the choice of an optimal length always involves a trade-off. The only way both the modulation depth and the footprint can be improved simultaneously, is by designing the waveguide so as to optimise the graphene-light interaction strength. The latter is known [16, 28, 29, 31] to be highly dependent on the location of the graphene layer relative to the optical mode, as the absorption is more efficient if graphene is placed

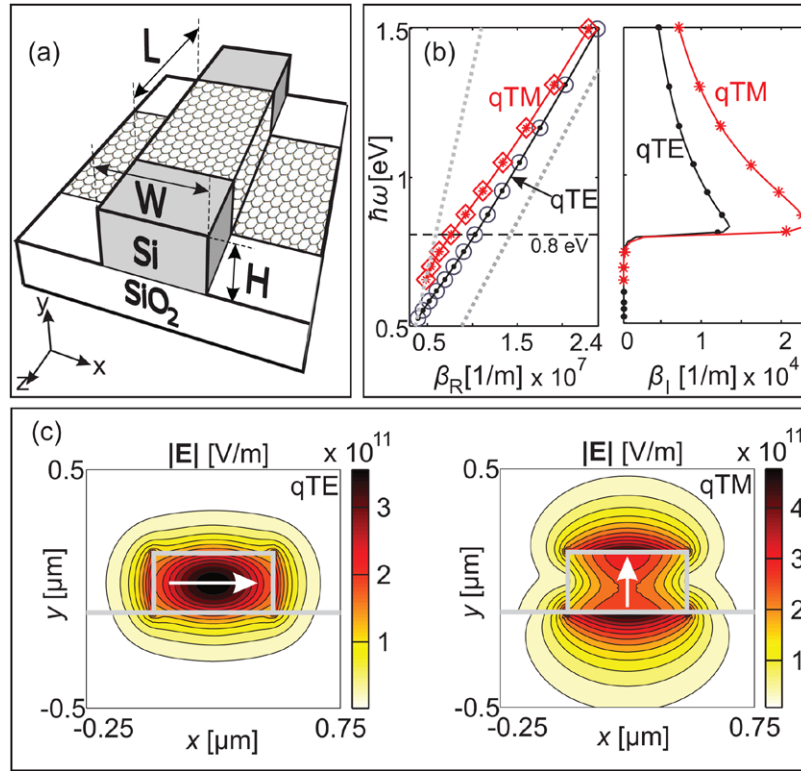


Figure 1. (a) Schematics of a graphene-coupled strip waveguide. (b) Real (left panel) and imaginary part (right panel) of dispersion relations for the fundamental qTE and qTM modes, obtained for $H = 0.25 \mu\text{m}$ and $W = 0.5 \mu\text{m}$. The empty and full markers represent the bare and graphene-coupled cases, respectively, while the dotted lines indicate the silicon and silica light lines. (c) The total electric field distribution at $\hbar\omega = 0.8 \text{ eV}$, as indicated by the dashed line in (b). The fields are normalised so that the modal energy per unit length U is equal to 1 J m^{-1} . The arrows show the dominant polarisation of the fields.

in the high-field region which is often in the middle of the waveguide [28]. While the fabrication of thin slots in silicon waveguides is possible [32] it is rather difficult and likely to decrease the waveguide quality. Thus, graphene is, in practice, deposited exclusively on the top of the waveguide [22–28].

Here we perform an eigenmode analysis implemented within the finite element method [33] to study how the geometrical parameters of a SOI strip waveguide affect the graphene-light interaction strength. The interpretation of the numerical results is done with the help of a perturbation approach, whose general properties and accuracy were the subject of our previous work [29]. Owing to the fact that the fields of optical eigenmodes are virtually unaffected by graphene [29], we find that: (i) the total absorption due to graphene segments placed at different locations along the waveguide cross section is additive, (ii) the modes of the bare and graphene-coupled waveguide are impedance-matched so the reflection on the entrance into the modulator is negligible and (iii) the ratio of the modulation depth (MD) and insertion losses (IL) does not depend on the waveguide and is determined solely by the optical properties of graphene, which indicates that the value close to 5 recently reported in [24] will be hard to improve upon. We also investigate whether there is a direct connection between the interaction strength and optical confinement [28] and find that the answer is negative, which is corroborated by a similar conclusion recently reached in attempts to maximise the graphene-induced nonlinear parameter [19]. Finally, we show that, in principle, by carefully choosing the waveguide

geometry, the modulation efficiency can be increased by up to several times.

2. The model: SOI waveguide-graphene system

Among various geometries being used in photonic integrated circuits, the so-called rib, buried and strip waveguides are the most common [20, 21]. Here we limit our attention to the case of strip waveguides, which have the highest index-contrast and for which single mode operation in the near-infrared can be obtained with submicron lateral dimensions [21]. We have found that the coupling strengths attainable with rib or buried waveguides are similar and can be analysed analogously. Figure 1(a) illustrates a SOI strip waveguide whose section of length L is covered by a layer of graphene.

The guided modes of a bare waveguide are classified into quasi-transverse electric (qTE) and quasi-transverse magnetic (qTM). The electric field of the former is polarised mainly horizontally (along the x -axis), while the latter is polarised mainly vertically (along the y axis), as shown by the example in figure 1(c). The propagation of modes along the z -axis is quantified by the propagation constant β , which is a purely real quantity in a bare waveguide with negligible losses.

Upon depositing graphene on the top of the waveguide, the propagation constant $\beta(\omega)$ of a guided mode at a given frequency ω is changed by $\Delta\beta(\omega)$. As graphene behaves both as a polarisable and absorptive system, $\Delta\beta(\omega)$ has both real and imaginary parts. Figure 1(b) shows the real part of dispersion

curves for the bare waveguide (circles-qTE, squares-qTM) and the dispersion curves for the graphene-coupled waveguide (lines with dots-qTE, lines with stars-qTM). In numerical calculations [33] of optical eigenmodes, the refractive indices for silicon ($n = 3.47$) and the silica substrate ($n = 1.44$) are taken to be real and constant, which is appropriate for the frequency range of around $\hbar\omega = 0.8$ eV, corresponding to the free-space wavelength of $\lambda = 1.55$ μm , which we focus on in this study. As the magnitude of $|\Delta\beta(\omega)|$ is of the order of 10^4 m^{-1} , the difference between the bare and graphene-coupled dispersion cannot be distinguished on the scale of figure 1(b) left panel. The right panel of figure 1(b) shows the imaginary part of the propagation constant for modes of the graphene-coupled waveguide.

In the calculations used in this study, graphene is represented by an infinitely thin layer having a frequency-dependent surface conductivity $\sigma(\omega)$. The simplest and most widely used model [34] for $\sigma(\omega)$ follows from the Kubo formalism in the non-interacting picture [35], in which $\sigma(\omega)$ is written as the sum of the interband

$$\sigma(\omega)_{\text{inter}} \approx \frac{iq^2}{4\pi\hbar} \ln \left(\frac{2E_F - \hbar(\omega + i\tau)}{2E_F + \hbar(\omega + i\tau)} \right), \quad (1)$$

and intraband conductivity

$$\sigma(\omega)_{\text{intra}} = \frac{iq^2 k_B T}{\pi \hbar^2 (\omega + i\tau)} \times \left[\frac{E_F}{k_B T} + 2 \ln \left(\exp \left(\frac{-E_F}{k_B T} \right) + 1 \right) \right]. \quad (2)$$

Here τ and T denote the electron relaxation rate and the temperature, while q is the elementary charge. The above model accounts for the main properties of graphene's linear optical response and its dependence on E_F , including the Drude-like behaviour at frequencies below $\hbar\omega = 2E_F$ (intraband transitions) and the flat absorption spectrum at frequencies above $\hbar\omega = 2E_F$ (interband transitions). This model, however, predicts that the residual conductance at frequencies slightly below the interband threshold frequency $\omega_{\text{th}} = 2E_F/\hbar$ is very close to zero. Experiments [3, 37, 38] have, however, shown that the residual conductance is $p\sigma_0$ with $\sigma_0 = q^2/4\hbar$ and p ranging from 0.3 to 0.5, depending on the graphene fabrication method and its electron concentration. Non-negligible values of p are known to be an inherent characteristic of graphene and a signature of many-body effects in its optical response [35, 36]. This fact is important for graphene-based modulators as p sets the lower bound on the insertion loss. Below we show that the modulation depth to insertion loss ratio is entirely independent on the waveguide geometry and is given by

$$\frac{\text{MD}}{\text{IL}} = \frac{1-p}{p}, \quad (3)$$

thus $\text{MD}/\text{IL} \approx 4.84$ reported in [24] implies $p \approx 0.17$, which is already quite small in comparison with values reported in spectroscopic studies of exfoliated graphene [35]. In view of the significance that taking a realistic dataset for $\sigma(\omega)$ has for

making meaningful numerical predictions, below we use the data reported in [3] modified as explained in [29] to account for various values of E_F . Meanwhile, the results shown in figure 1 are obtained with the use of equations (1) and (2) with $T = 300$ K, $\tau = 1.77 \times 10^{-13}$ s and $E_F = 0.4$ eV.

We note here that the conducting sheet model [34] of graphene employed in our calculations is equivalent to an anisotropic thin film model [39] in which graphene is represented as a thin film of thickness $d_g \approx 0.34$ nm and relative permittivity components

$$\epsilon_{\parallel}(\omega) = 1 + \frac{i\sigma(\omega)}{d_g \omega \epsilon_0}, \quad \epsilon_{\perp} = \epsilon_b, \quad (4)$$

that differ for dielectric response parallel ($\epsilon_{\parallel}(\omega)$) and perpendicular (ϵ_{\perp}) to the graphene layer. Here ϵ_b denotes the background permittivity (in our case equal to unity for air) indicating that graphene carriers cannot respond to the electric field component \mathbf{E}_{\perp} perpendicular to the sheet. The equivalence between the conducting sheet and thin film model is a simple consequence of the fact that all the involved wavelengths are several orders of magnitude longer than d_g . Modeling graphene by the use of isotropic values for its permittivity $\epsilon(\omega) = \epsilon_{\parallel}(\omega)$ can lead to erroneous results in cases where \mathbf{E}_{\perp} is not negligible. This is particularly important at frequencies such that $\epsilon(\omega) \approx 0$ (the bulk plasma frequency of the hypothetical medium), for which the isotropic model predicts a spurious enhancement of \mathbf{E}_{\perp} within the fictitious thin film, by means of a mechanism akin to the one used in reducing the mode volume in dielectric optical microcavities [40]. This can further lead to large spurious graphene absorption rates, as evidenced by some of the unrealistically high values reported in the literature.

At frequencies in the vicinity of ω_{th} , where these modulators are operated, the magnitude of $\sigma(\omega)$ can reach $3\sigma_0$ – $4\sigma_0$ at most. This is found to be insufficient to noticeably modify the field distribution of any of the considered guided modes. For example, the electric fields in figure 1(c) drawn for the bare waveguide are virtually identical to the fields in the graphene-coupled waveguide. In fact, we find that the situation in strip waveguides is similar to the case of planar waveguides examined in [29], where it was found that magnitudes of $|\sigma(\omega)|$ as high as $30\sigma_0$ are required in order to visibly disturb the fields. An important practical consequence of this is that graphene-based modulators are always impedance-matched to the bare waveguide.

We now introduce a quantitative measure for the graphene-waveguide coupling strength. Starting from the graphene-coupled waveguide but replacing $\sigma(\omega)$ by an infinitesimally small conductance $\Delta\sigma$, the bare waveguide dispersion $\beta(\omega)$ of a given mode is retrieved as $\Delta\sigma \rightarrow 0$. A nonzero but very small $\Delta\sigma$ will modify the propagation constant by $\Delta\beta(\omega)$, which, to the first order, is proportional to $\Delta\sigma$. We thus define the graphene-waveguide coupling strength $G(\omega)$ as the derivative:

$$G(\omega) = -i \frac{d\beta(\omega)}{d\sigma}, \quad (5)$$

with the $-i$ multiplier introduced for convenience (it makes $G(\omega)$ almost entirely real, as shown below) and where $d\sigma$ can

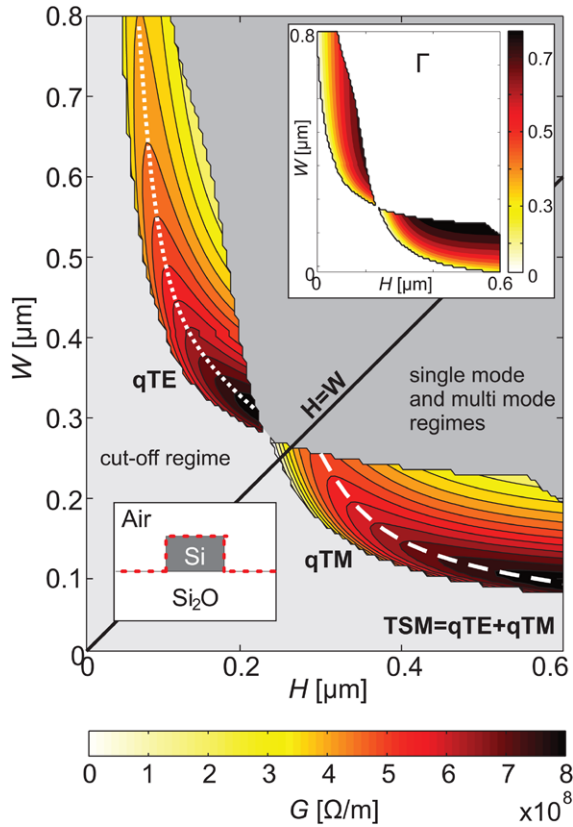


Figure 2. Greyscale (colour) map of G calculated at $\lambda = 1.55 \mu\text{m}$ for the structure shown in the lower inset (the graphene layer is represented by the thick dotted line). The upper inset shows the corresponding mode confinement factors Γ .

have an arbitrary phase. In case $|\sigma|$ becomes sufficiently larger than zero, so that $d\beta(\omega)/d\sigma$ evaluated at $\sigma = 0$ is significantly different from the derivative evaluated at $|\sigma| > 0$, the coupling strength should be considered as a function of both conductivity and frequency. However, according to [29], this would typically require values of $|\sigma|$ larger than $30\sigma_0$, which is much higher than the conductance of a single or few layer graphene at these frequencies. Considering that graphene practically does not change the electromagnetic fields, we may invoke the perturbation theory [41] to show that

$$\Delta\beta(\omega) \approx i\sigma(\omega)G(\omega), \quad (6)$$

i.e. that the simple proportionality between $\Delta\beta$ and σ holds for all magnitudes of σ relevant for graphene modulators at telecommunication wavelengths [29]. Furthermore, it follows that $G(\omega)$ can be, to an excellent approximation and for a wide range of relevant parameters [29], written in terms of bare waveguide eigenmodes

$$G(\omega) \approx \frac{1}{4v_g(\omega)U(\omega)} \int_{\text{graph}} |\mathbf{E}_{\parallel}|^2 dl, \quad (7)$$

with $U(\omega)$ and $v_g(\omega)$ denoting the bare modal energy per unit length (along the z -axis) and group velocity, respectively. The integral of the electric field component \mathbf{E}_{\parallel} parallel to the graphene sheet is taken along all the lines in the waveguide cross section which correspond to boundaries covered by graphene. Equation (7) shows that only electric field components parallel

to the graphene layer can lead to absorption, and also that the total absorption in separate graphene patches is always additive, which is used below for analysing the contribution of individual waveguide boundaries to $G(\omega)$.

3. Results and discussion

3.1. Analysis of the graphene-guided mode coupling strength

The coupling strength introduced above is, evidently, a characteristic of the mode being propagated in the waveguide. Here we focus on waveguides operated in the true single mode (TSM) regime, defined as the regime in which exactly one mode (qTE or qTM) is allowed to propagate at the operating frequency $\hbar\omega_{\text{op}} = 0.8 \text{ eV}$. The quantity denoted below by G refers to the coupling strength of the appropriate mode with graphene at $\omega \approx \omega_{\text{op}}$. In contrast to TSM, the term single mode regime is used in the literature [21] for cases in which the waveguide supports either only one mode, or two modes but with orthogonal polarisations (the lowest qTE and qTM modes).

Figure 2 shows the greyscale (colour) map of G as a function of the silicon strip height H and width W , calculated for a waveguide entirely covered by graphene (as sketched by the bottom-left inset) within a part of the H – W parametric plane that belongs to the TSM regime. The latter comprises two disjoint regions denoted by qTE (upper left) and qTM (lower right), representing the H – W values for which the fundamental mode is qTE and qTM, respectively, while higher modes are not allowed. The qTE and qTM regions in figure 2 would be symmetric across the $H = W$ curve, if it not were for the silica substrate. Since the silica refractive index ($n = 1.44$) is higher than the refractive index of air, the horizontally polarised modes are slightly red-shifted relative to their vertically polarised counterparts, which causes the qTM region to slightly spill over into the $W > H$ half-plane. This further implies that in the close vicinity of the $H = W$ curve in the TSM regime, the modes always belong to the qTM polarisation. As the fundamental cutoff frequency increases when decreasing either H or W , the part of the H – W plane below and to the left of the TSM region corresponds to waveguides in which no mode is allowed to propagate at $\omega \approx \omega_{\text{op}}$. And vice-versa, the part of the H – W plane above and to the right of the TSM greyscale (colour) map represents the waveguides supporting at least two modes at $\omega \approx \omega_{\text{op}}$.

We find from figure 2 that the qTE modes have very efficient coupling with the graphene layer for waveguide geometries near the $H = W$ curve. In the case of qTM modes, high values of G are reached further away from the $H = W$ curve, increasing even further for heights beyond the range shown in figure 2. Such a high aspect ratio waveguide cross section is, nevertheless, likely to be irrelevant in practice due to fragility and difficulties in fabrication. Additionally, the detachment of graphene from vertical boundaries might also become considerable, decreasing significantly the overall value of G , as shown in section 3.3. In the plotted H – W range, the qTE G map has a maximum at around $H \approx 0.22 \mu\text{m}$ and $W \approx 0.31 \mu\text{m}$, whereas the qTM region maximum is at $H \approx 0.6 \mu\text{m}$ and

Table 1. Parameters of the maxima lines for the qTE and qTM modes.

Parameters	a	b	c
qTE	0.001 444	2.267	0.2734
qTM	0.004 906	3.007	0.075 45

$W \approx 0.1 \mu\text{m}$. These maxima are located near the very end of the TSM regime for both modes. However, a variation of H or W of around 20 nm from the mentioned coordinates, within the TSM regime, induces a change of less than 2% in the maximal values of G , indicating that the benefit obtained by geometric optimisation can be reliably transferred into fabricated devices.

For any given H , there is a single value of W for which G reaches a maximum. The dotted and dashed lines in figure 2 connecting these maxima are found to be well parameterised by the following curve

$$W = \frac{a}{H^b} + c, \quad (8)$$

with a , b and c , listed in table 1, for both qTE and qTM regions. Note that the fit parameters in equation (8) correspond to H and W values expressed in microns.

The existence of such extremal points within the TSM regime is a direct proof that the graphene-waveguide coupling strength cannot simply be expressed in terms of the mode confinement factor Γ . To show this, we introduce Γ as the ratio of the power carried within the silicon strip, to the total mode power, i.e. as

$$\Gamma = \frac{\int_{\text{Si}} P_z dx dy}{\int_{\text{Si}} P_z dx dy + \int_{\text{SiO}_2} P_z dx dy + \int_{\text{air}} P_z dx dy}, \quad (9)$$

where P_z denotes the z -component of the time-averaged Poynting vector. We find in the upper-right inset in figure 2 that, as expected, Γ increases monotonously with increasing both H and W , i.e. with moving away from the cut-off regime. Since the graphene layer covers the outer boundaries of the waveguide, at first it might appear that modes which are less confined will have a higher G . However, this is not what is seen in figure 2, which shows that G actually decreases to zero at the boundaries between TSM and the cut-off regime. Furthermore, going along the extremal (dotted and dashed) lines in figure 2 shows that reducing the width of the waveguide and increasing its height according to equation (8) improves the graphene coupling efficiency of both modes, regardless of their being more or less confined.

3.2. Contribution of individual boundaries

We have seen in equation (7) in section 2 that, owing to the small effect graphene has on the fields, the total value of G can be considered to originate from the sum of individual contributions of each waveguide boundary covered by graphene. Since the waveguide is symmetric across the $y-z$ plane, we may write

$$G = 2G_1 + 2G_2 + G_3. \quad (10)$$

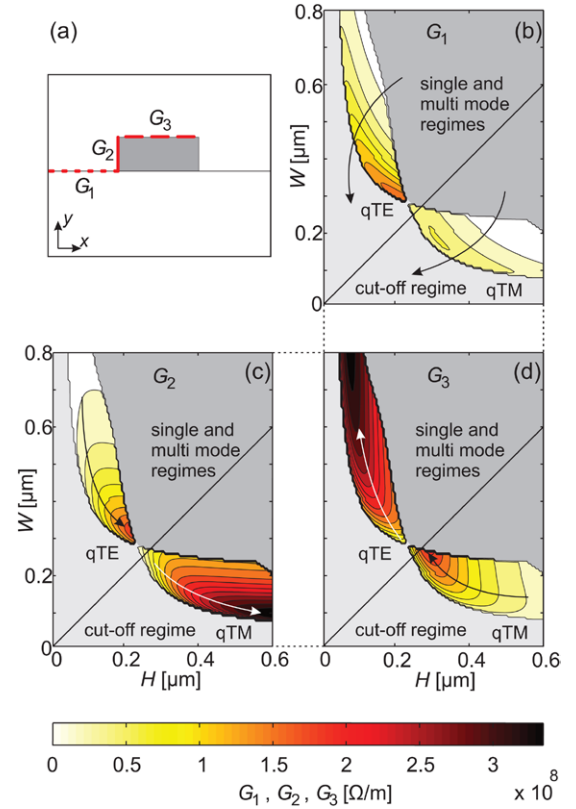


Figure 3. (a) Illustration showing graphene layers which are deposited on the lower horizontal (dotted line), vertical (solid line) and top horizontal (dashed line) boundaries of the waveguide. (b) Greyscale (colour) map of G_1 corresponding to the graphene on lower horizontal boundary. (c) Greyscale (colour) map of G_2 corresponding to the graphene on vertical boundary. (d) Greyscale (colour) map of G_3 corresponding to the graphene on top horizontal boundary. The arrows show the direction in which G_1 , G_2 and G_3 are increasing.

Here G_1 represents the coupling strength between the waveguide and graphene placed at the horizontal boundary separating the oxide layer and air. Similarly, G_2 and G_3 are coupling strengths for graphene at the vertical and horizontal boundaries between the Si wire and air, respectively. The segments corresponding to the definition of G_1 , G_2 and G_3 are sketched in figure 3(a) with dotted, solid and dashed lines, respectively. The remainder of figure 3 shows the greyscale (colour) maps of G_1 , G_2 and G_3 for the same $W-H$ range as considered in figure 2. To facilitate the comparison, the (b)–(d) panels in figure 3 share their H and W axes and have the same greyscale (colour) bar located at the bottom of figure 3.

The arrows in figure 3(b) show that G_1 increases when going from the single and multi-mode towards the cut-off regime. The strongest coupling is reached for geometries near the $H = W$ curve. Comparing the two polarisations, the qTM mode is seen to couple less efficiently. This is because the E_x and E_z electric field components, parallel to the boundary between the substrate and air on which the assumed graphene ribbon is deposited (see figure 3(a)), are stronger for the qTE polarisation. The main characteristics of the electric fields for the qTE and qTM modes for several geometries along the extremal points defined by equation (8) are given in figures 4

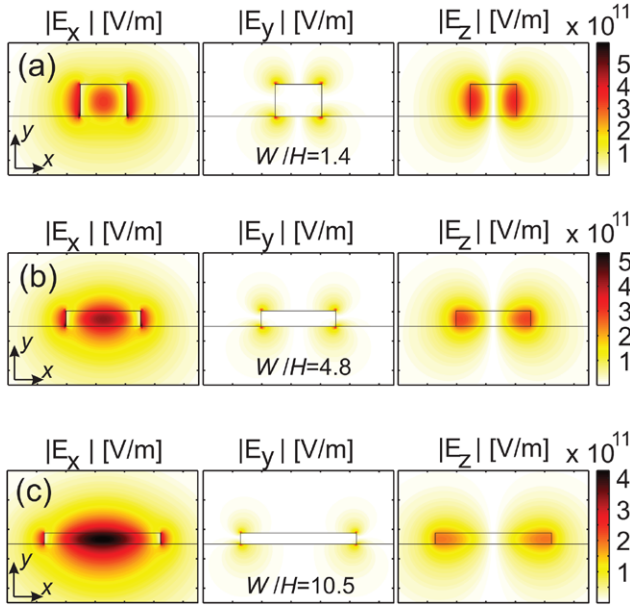


Figure 4. (a) qTE electric field components, for $H \approx 0.22 \mu\text{m}$ and $W \approx 0.31 \mu\text{m}$. (b) qTE electric field components, for $H \approx 0.105 \mu\text{m}$ and $W \approx 0.51 \mu\text{m}$. (c) qTE electric field components, for $H \approx 0.075 \mu\text{m}$ and $W \approx 0.79 \mu\text{m}$. Shown electric field components are normalised so that $U = 1 \text{ J m}^{-1}$.

and 5, respectively. The three geometries for both polarisations correspond to the starting, middle and ending points of the corresponding extremal curves. The fields intensities represented by the greyscale (colour) maps in figures 4 and 5 are all normalised so that the mode energy per unit length appearing in equation (7) equals unity, i.e. $U = 1 \text{ J m}^{-1}$.

By examining figure 3(c), we find that qTM mode couples with graphene on the vertical boundary more efficiently when the H/W ratio is increased, as shown by the arrows. This is understood by analysing how the electric field components E_y and E_z of the corresponding modes, as shown in figure 5, change when H and W are varied. As H is increased the amount by which these field components overlap the vertical boundary becomes larger. Furthermore, shrinking the width of the waveguide leads to the field delocalisation and the intensity of the E_y and E_z components grows at the vertical boundaries. Hence the qTM mode has the strongest coupling with graphene on this boundary for $H \approx 0.6 \mu\text{m}$ and $W \approx 0.1 \mu\text{m}$. The qTE mode couples more efficiently with graphene on the vertical edges than the qTM mode for geometries near $H = W$ curve. Here, the E_z field component of the qTE mode dominates the coupling efficiency since the E_y component is small, as seen in figure 4. On decreasing the width of the waveguide while increasing the height, the E_z maxima move away from the centre of the waveguide and towards the boundaries of the Si wire. This can be seen by comparing E_z in figures 4(a)–(c). Furthermore, the amount of overlapping of E_z component with the graphene ribbon on the vertical boundary becomes higher as the height grows. Thus the most efficient coupling, for the qTE mode, is obtained at $H \approx 0.22 \mu\text{m}$ and $W \approx 0.31 \mu\text{m}$.

Figure 3(d) shows that if just the top horizontal boundary is covered by graphene, the qTE mode-graphene coupling would be maximized by decreasing the height and increasing

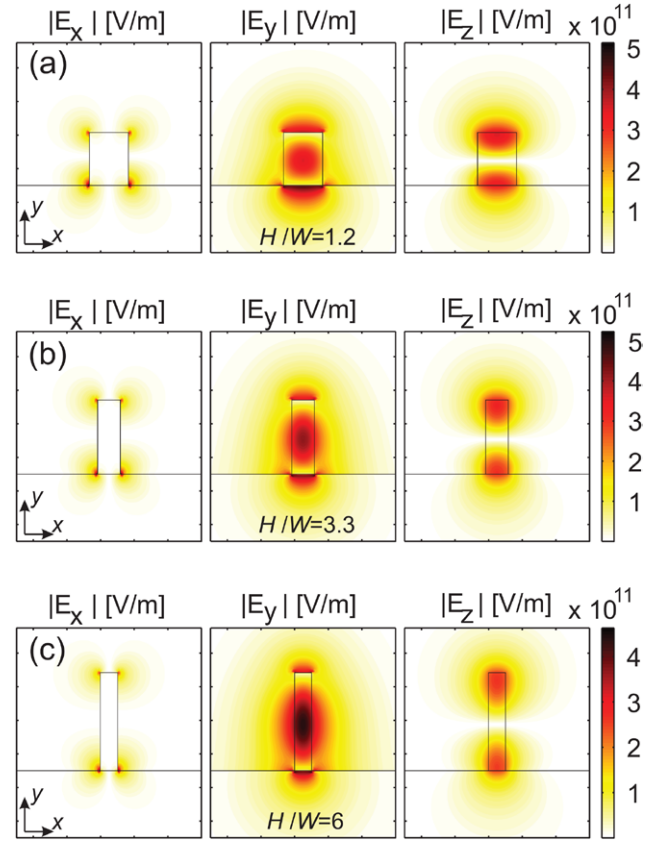


Figure 5. (a) qTM electric field components, for $H \approx 0.3 \mu\text{m}$ and $W \approx 0.25 \mu\text{m}$. (b) qTM electric field components, for $H \approx 0.44 \mu\text{m}$ and $W \approx 0.135 \mu\text{m}$. (c) qTM electric field components, for $H \approx 0.6 \mu\text{m}$ and $W \approx 0.1 \mu\text{m}$. The shown electric field components are normalised so that $U = 1 \text{ J m}^{-1}$.

the width of the waveguide, as indicated by the arrows. This behaviour, opposite to the case of the vertical waveguide boundary, is also understood by considering the E_x and E_z components of the qTE mode in figure 4, which become less localised and stronger on the top horizontal boundary as the W/H ratio is increased. In the case of the qTM mode, the E_z component in figure 5 mainly contributes to the overall coupling since the E_x component is very small. Thus, lowering the H/W ratio leads to the movement of the E_z maxima towards the horizontal boundaries of the Si wire, and consequently to a stronger interaction of the qTM mode with the graphene layer covering the top horizontal boundary. Also, higher values of W imply that E_z has a better overlap with the graphene on this boundary. The most efficient coupling, for the qTE mode, is obtained at $H \approx 0.075 \mu\text{m}$ and $W \approx 0.79 \mu\text{m}$ and for the qTM mode at $H \approx 0.3 \mu\text{m}$ and $W \approx 0.25 \mu\text{m}$.

Finally, figures 3(b)–(d), can be used to explain figure 2, i.e. the graphene-waveguide coupling strength in case the graphene covers the entire waveguide. For geometries with a high W/H ratio the most influential is the graphene segment covering the top horizontal boundary of the Si wire. When the W/H ratio is decreased the influence of the graphene covering the vertical and lower horizontal boundaries becomes more significant. The maximum in the qTE-G map is actually due to coupling between the mode and graphene layer on the vertical

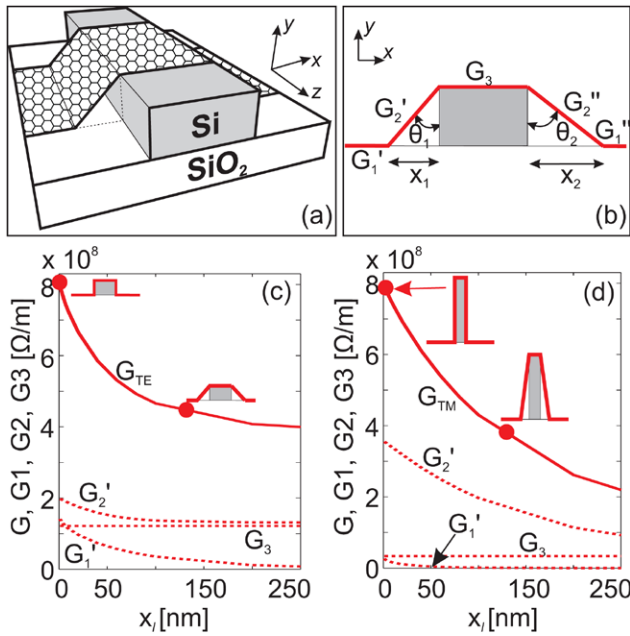


Figure 6. (a) Sketch of a graphene-waveguide structure in which the graphene is completely detached from the vertical waveguide boundaries. (b) Cross-section of the waveguide in (a) used to define the displacements x_1 and x_2 , and angles θ_1 and θ_2 . (c) The total coupling strength G_{TE} and its G'_1 , G'_2 and G_3 components, calculated for a waveguide having $H \approx 0.22 \mu\text{m}$ and $W \approx 0.31 \mu\text{m}$ (d) G_{TM} and its components G'_1 , G'_2 and G_3 , calculated for a waveguide having $H \approx 0.6 \mu\text{m}$ and $W \approx 0.1 \mu\text{m}$.

boundaries. In the case of the qTM mode for the (H, W) pairs near the $H = W$ curve the graphene on the top horizontal boundary mainly contributes to the overall coupling with this mode.

3.3. Decrease in coupling strength due to detachment from the vertical boundaries

So far, we have assumed that graphene conforms perfectly to all of the waveguide boundaries that it might cover. In practice, however, graphene might not be attached ideally to the vertical boundaries. Here we assess what impact this might have on G . Figure 6(a) illustrates an augmented case of the graphene layer being detached from the vertical boundaries, which can be quantified by displacements x_1 , x_2 , and angles θ_1 , θ_2 , as sketched in figure 6(b).

As before, the total coupling strength can be expressed as a sum of contributions from an individual graphene segment, as shown in figure 6(b)

$$G = G'_1 + G'_2 + G_3 + G''_2 + G''_1, \quad (11)$$

where G'_1 , G'_1 and G_3 represent the coupling between the waveguide and graphene at the horizontal boundaries, while G'_2 and G''_2 represent the coupling between the waveguide and the slanted segments. For simplicity, we assume $\theta_1 = \theta_2 = \theta$ and $x_1 = x_2 = x_l$ so that $G'_1 = G''_1$ and $G'_2 = G''_2$.

In section 3.2, we have shown that the coupling between the waveguide and graphene is dominated by the contributions of the graphene segments at the top, horizontal and vertical

boundaries. Therefore, it is expected that, for a fixed waveguide geometry, the value of G would be modified mainly due to the modification of G'_2 as θ increases from zero.

Figures 6(c) and (d) show the variation of the total coupling strength with x_l for the two waveguides from section 3.1 having the most efficient coupling with graphene and whose electric field components have been given in figures 4(a) and 5(c). For $x_l = 0$, the graphene conforms ideally to the vertical boundaries, and G is the same as the one in figure 2 for the qTE and qTM modes shown in figures 6(c) and (d), respectively. As x_l increases, both G_{TE} and G_{TM} are seen to decrease. This can be explained by analysing the G'_1 , G'_2 and G_3 components shown as dotted lines in figures 6(c) and (d). G_3 does not depend on x_l (see figure 6(b)) and hence it is constant throughout the considered displacement range. On the other hand, displacing the graphene away from the vertical boundaries yields lower values of G'_1 and G'_2 . This is due to the rapid decay of the corresponding electric field components outside of the waveguide. In the case of the qTM mode, G'_2 is the one that determines the modification of G_{TM} , as expected. However, for the qTE mode, both G'_1 and G'_2 affect the trend in G_{TE} . The steep initial decrease of both G_{TE} and G_{TM} as x_l increases from zero shows that even displacements of around 10 nm can noticeably modify the coupling efficiency, meaning that the conformity of the graphene layer on the silicon waveguide is an important aspect to consider in designing graphene-based optical modulators. The comparison of figures 6(c) and (d) shows that the small aspect ratio waveguides carrying the qTE modes are much more robust to graphene detachment issues than the high aspect ratio qTM waveguides.

3.4. Influence of the coupling strength on the optical properties of electro-absorptive optical modulators

Having seen how the geometrical parameters of the waveguide influence the coupling between the given mode and the graphene layer over a specific boundary, we now consider how it affects the operation of electro-absorptive modulators. The power transmittance through a graphene-coupled waveguide segment of length L is determined by the imaginary part β_I of the optical propagation constant, which is equal to $\Delta\beta_I$. Therefore, the transmittance expressed in dB and per unit length of the waveguide becomes

$$T_r[\text{dB m}^{-1}] = -\frac{20}{\ln 10} \Delta\beta_I. \quad (12)$$

Figure 7 shows T_r expressed in $[\text{dB } \mu\text{m}^{-1}]$ versus the position of the Fermi level in graphene, evaluated at $\hbar\omega_{\text{op}} = 0.8 \text{ eV}$ ($\lambda = 1.55 \mu\text{m}$) for two representative waveguide geometries. The value of E_F is assumed to be varied by applying a gate voltage on graphene, which can be done in several ways [22–27], perhaps the use of two graphene layers on top of each other being the most effective [23, 24, 27]. While the choice of any particular solution for introducing the gating on graphene will affect the optical properties of the waveguide to some extent, the part of the analysis that is relevant for modulation will always be the same. Thus, although the conclusions below are reached on a simplified system, it is easily seen that

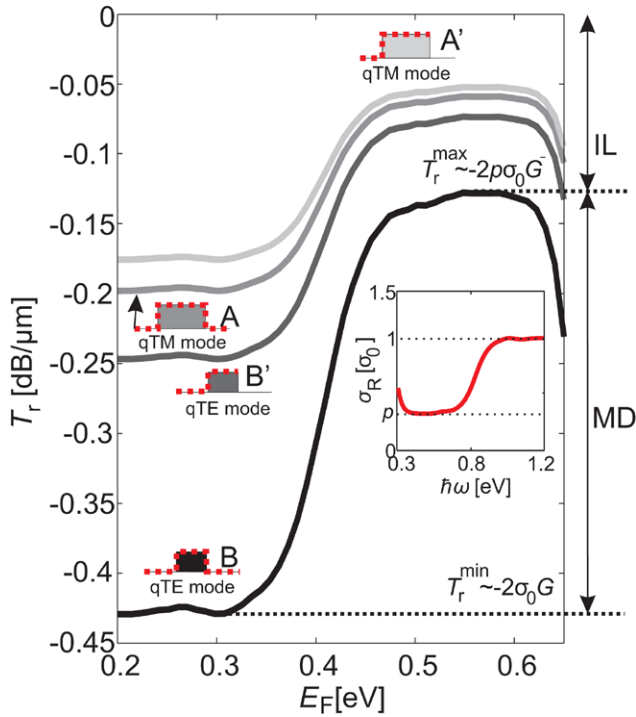


Figure 7. Transmittance versus the position of the Fermi level in graphene for four different modulators. They are illustrated near their corresponding transmittance curves. A and A' modulators have $H = 0.25 \mu\text{m}$ and $W = 0.6 \mu\text{m}$, and are entirely and partially covered by graphene, respectively. B and B' modulators have $H \approx 0.22 \mu\text{m}$ and $W \approx 0.31 \mu\text{m}$, and are entirely and partially covered by graphene, respectively. The maximal and minimal value of the transmittance, MD and IL are shown using the B modulator's curve. The inset shows σ_R in units of σ_0 with the minimal and maximal values defined by the dotted lines.

they are equally applicable to the general case. In order to have as realistic predictions as possible, here the $\sigma_R(\omega)$ values reported in [3] for a gate voltage of 71 V ($E_F \approx 0.29 \text{ eV}$) were used. In the absence of experimental data on $\sigma_R(\omega)$ beyond $E_F \approx 0.29 \text{ eV}$, the experimental dataset $\sigma_R(\omega)$ was shifted to cover all E_F values in the immediate vicinity $\hbar\omega_{\text{op}}/2 = 0.4 \text{ eV}$, as in [29]. The $T_r(E_F)$ curves shown in figure 7 are obtained by calculating the propagation constant of the waveguide with graphene. However, owing to the mentioned accuracy of the perturbative expressions, we find that they are identical with the curves obtained using $G(\omega)$ evaluated from equations (7) and (6).

As a comparison with previous work, we consider a waveguide, denoted by A, which has $H = 0.25 \mu\text{m}$, $W = 0.6 \mu\text{m}$, corresponding to the one studied in [22]. The 7 nm thick Al_2O_3 layer that was used in [22] to electrically insulate graphene from the semiconducting silicon strip is neglected in our comparison for clarity. Taking this thin layer into account leads only to small modifications of the G value, which are of the order of a few per cent for the considered waveguides, and it thus does not affect our analysis. For example, direct calculations show that if a 7 nm thick Al_2O_3 layer is added between graphene and waveguide A, the G value of the considered TM mode would decrease by about 5%. As the second waveguide, denoted by B, we consider the waveguide with $H \approx 0.22 \mu\text{m}$

and $W \approx 0.31 \mu\text{m}$, which is one of the geometries for which we have found above to couple strongly to graphene (the one having the highest G for qTE). A comparison of waveguide A parameters with figures 2 and 3 shows that, at the chosen operating frequency, waveguide A is not in the TSM regime that we have focused our attention to. Instead, it is found to support three modes at $\hbar\omega_{\text{op}}$. Here we evaluate its properties for the qTM mode, which is the mode that has been utilised in the experiments in [22]. Two possible cases of graphene deposition are evaluated. By A and B we denote the modulators obtained when the waveguides are covered entirely by graphene, as indicated by the thick (red) dotted lines in figure 7 insets. A' and B', on the other hand, represent the modulators in which the waveguides are covered only partially, as also indicated by the figure 7 insets. Modulator A' is, actually, the configuration that has been studied in [22].

The key quantities describing a modulator are modulation depth (MD) and insertion loss (IL). When transmittance is expressed in dB and per unit length of the waveguide, MD is defined as the difference of the maximum and minimum values of the transmittance, while IL represents the amount by which the transmittance is decreased as a result of introducing graphene. These two quantities are illustrated in figure 7 on the example of waveguide B. Using equation (6) and considering how $\sigma_R(\omega)$ behaves in the vicinity of the interband threshold frequency (see the figure 7 inset), we find that there is a simple relationship between the coupling constant $G(\omega_{\text{op}})$ at the operating frequency and p , which quantifies the residual conductivity of graphene discussed in section 2

$$\text{MD}[\text{dB m}^{-1}] \approx -\frac{20}{\ln 10}(1-p)\sigma_0 G(\omega_{\text{op}}), \quad (13)$$

and

$$\text{IL}[\text{dB m}^{-1}] \approx -\frac{20}{\ln 10}p\sigma_0 G(\omega_{\text{op}}). \quad (14)$$

Thus, by dividing equations (13) and (14), we recover the mentioned fact, stated by equation (3), that the ratio of MD to IL is independent of the waveguide geometry and determined entirely by the residual conductivity of graphene. This is also seen in figure 7, where the modulators with a higher MD are seen to have a proportionally higher IL. In this particular case, the values [3] of $\sigma(\omega)$ used in calculations imply $p \approx 0.3$, which amounts to $\text{MD}/\text{IL} \approx 2.33$. It should be noted that equations (13) and (14), and consequently equation (3), rely on two important characteristics of the considered graphene-waveguide system, which are: (1) The graphene-waveguide coupling strength, G , depends only on frequency, as explained in section 2. (2) The mode propagation losses of the bare waveguide are negligible in comparison with the losses induced by residual conductance. This is generally true for SOI waveguides, which have small propagation losses at telecommunication wavelengths [42].

In figure 7, the highest modulation depth of $0.3 \text{ dB } \mu\text{m}^{-1}$ is reached for modulator B. Both modulators A and A', corresponding to the one given in [22], are seen to have more than two times smaller MDs. The difference in coupling strength and thus in MDs between A and A' is not very big

and, obviously, results from A having a higher graphene coverage than A'. A comparison of $T_r(E_F)$ for the four modulators clearly shows that the amount by which the waveguide is covered by graphene is not the only factor which determines the MD. It is rather the appropriate choice of the geometry for the given mode's polarisation that determines how high the MD will be. Here we see that the B' modulator has a higher MD, even though it has a smaller graphene coverage. Thus, our analysis demonstrates that by a wise choice of SOI waveguide parameters, the graphene-waveguide coupling constant can be increased by up to a few times.

4. Summary

We have shown how the variation of the strip width and height in SOI strip waveguides can be used to increase the graphene-waveguide coupling strength G . The values of G for practically all the relevant waveguide width and height pairs have been evaluated showing that over the entire parameter plane, the value of G changes up to few times.

As tailoring the geometry of a waveguide and the graphene ribbon deposited on it always involves considering additional constraints, such as the issue of gating graphene, it is important to understand how covering only parts of the waveguide affects the coupling strength. We have shown that the effect of disjoint graphene patches is always additive and then used this fact to analyse from which graphene segments most of the coupling efficiency originates. For example, we have found that in the case of complete waveguide coverage by graphene, the most efficient coupling is reached for the qTE mode, in a waveguide with $H \approx 0.22 \mu\text{m}$ and $W \approx 0.31 \mu\text{m}$ yielding a modulator with $\text{MD} \approx 0.3 \text{ dB } \mu\text{m}^{-1}$, which is estimated to be almost three times higher than the value reported in a previous study [22]. Interestingly, for this (H, W) pair, a very large relative contribution comes from graphene on the vertical boundaries of the silicon wire, which is somewhat unexpected since the qTE modes are mainly horizontally polarised.

Our analysis has also shown that the value of G depends on how well the graphene layer conforms to the waveguide surface and that it cannot be simply related to the mode confinement factor. In particular, we have found that the local maxima of G follow two distinct curves within the true single mode regime.

We have also shown that the ratio of the modulation depth to insertion losses, which is a commonly used figure of merit for electro-optical modulators, does not depend on the waveguide geometry and graphene coverage at all, but that it is exclusively a function of the residual conductivity of graphene.

Acknowledgments

This work was funded by the Serbian Ministry of Education, Science and Technological Development under Projects No. OI171005 and No. OI171011. The authors are also grateful for support by the European Community's 7th Framework Programme under Grant Agreement No. 228637 NIMNIL.

References

- [1] Novoselov K S, Geim A K, Morozov S V, Jiang D, Zhang Y, Dubonos S V, Grigorieva I V and Firsov A A 2004 *Science* **306** 666
- [2] Nair R R, Blake P, Grigorenko A N, Novoselov K S, Booth T J, Stauber T, Peres N M R and Geim A K 2008 *Science* **320** 1308
- [3] Li Z Q, Henriksen E A, Jiang Z, Hao Z, Martin M C, Kim P, Stormer H L and Basov D N 2008 *Nat. Phys.* **4** 532
- [4] Wang F, Zhang Y, Tian C, Girit C, Zettl A, Crommie M and Shen Y R 2008 *Science* **320** 206
- [5] Novoselov K S, Geim A K, Morozov S V, Jiang D, Katsnelson M I, Grigorieva I V, Dubonos S V and Firsov A A 2005 *Nature* **438** 197
- [6] Koester S J, Li H and Li M 2012 *Opt. Express* **20** 20330
- [7] Bao Q and Loh K P 2012 *ACS Nano* **6** 3677
- [8] Bonaccorso F, Sun Z, Hasan T and Ferrari A C 2010 *Nat. Photonics* **4** 611
- [9] Geim A K and Novoselov K S 2007 *Nat. Mater.* **6** 183
- [10] Novoselov K S, Fal'ko V I, Colombo L, Gellert P R, Schwab M G and Kim K 2012 *Nature* **490** 192
- [11] Vakil A and Engheta N 2011 *Science* **332** 1291
- [12] Kim K, Choi J-Y, Kim T, Cho S-H and Chung H-J 2011 *Nature* **479** 338
- [13] He X-J, Li T-Y, Wang L, Wang J-M, Jiang J-X, Yang G-H, Meng F-Y and Wu Q 2014 *J. Appl. Phys.* **115** 17B903
- [14] Gan X *et al* 2013 *Nano Lett.* **13** 691
- [15] Vasic B and Gajic R 2014 *Opt. Lett.* **39** 6253
- [16] Lu Z and Zhao W 2012 *J. Opt. Soc. Am. B* **29** 1490
- [17] Gosciński J and Tan D T H 2013 *Nanotechnology* **24** 185202
- [18] Gruhler N, Benz C, Jang H, Ahn J-H, Danneau R and Pernice W H P 2013 *Opt. Express* **21** 31678
- [19] Donnelly C and Tan D T H 2014 *Opt. Express* **22** 22820
- [20] Knights A P and Reed G T 2004 *Silicon Photonics: an Introduction* (Chichester: Wiley)
- [21] Reed G T 2008 *Silicon Photonics: the State of the Art* (Chichester: Wiley)
- [22] Liu M, Yin X, Ulin-Avila E, Geng B, Zentgraf T, Ju L, Wang F and Zhang X 2011 *Nature* **474** 64
- [23] Liu M, Yin X and Zhang X 2012 *Nano Lett.* **12** 1482
- [24] Mohsin M, Schall D, Otto M, Nocolak A, Neumaier D and Kurz H 2014 *Opt. Express* **22** 15292
- [25] Youngblood N, Anugrah Y, Ma R, Koester S J and Li M 2014 *Nano Lett.* **14** 2741
- [26] Li H, Anugrah Y, Koester S J and Li M 2012 *Appl. Phys. Lett.* **101** 111110
- [27] Koester S J and Li M 2012 *Appl. Phys. Lett.* **100** 171107
- [28] Koester S J and Li M 2014 *IEEE J. Sel. Top. Quantum* **20** 6000211
- [29] Ralević U, Isic G, Vasic B and Gajic R 2014 *J. Phys. D: Appl. Phys.* **47** 335101
- [30] Sodagar M, Moradinejad H, Eftekhari A A and Adibi A 2014 *Opt. Lett.* **39** 4545–8
- [31] Gosciński J and Tan D T H 2013 *Sci. Rep.* **3** 1
- [32] Martinez A *et al* 2010 *Nano Lett.* **10** 1506
- [33] COMSOL 2015 *Version 4.4* www.cousol.com
- [34] Hanson G W 2008 *J. Appl. Phys.* **103** 064302
- [35] Basov D N, Fogler M M, Lanzara A, Wang F and Zhang Y 2014 *Rev. Mod. Phys.* **86** 959
- [36] Tassin P, Koschny T, Kafesaki M and Soukoulis C M 2012 *Nat. Photonics* **6** 259
- [37] Horng J *et al* 2011 *Phys. Rev. B* **83** 165113
- [38] Yan H, Xia F, Zhu W, Freitag M, Dimitrakopoulos C, Bol A A, Tulevski G and Avouris P 2011 *ACS Nano* **5** 9854
- [39] Mousavi S H *et al* 2013 *Nano Lett.* **13** 1111
- [40] Robinson J T, Manolatu C, Chen L and Lipson M 2005 *Phys. Rev. Lett.* **95** 143901
- [41] Isic G, Gajic R and Vukovic S 2014 *Phys. Rev. B* **89** 165427
- [42] Vlasov Y and McNab S 2004 *Opt. Express* **12** 1622